

## Spatial inhomogeneity and strong correlation physics: A dynamical mean-field study of a model Mott-insulator–band-insulator heterostructure

Satoshi Okamoto and Andrew J. Millis

*Department of Physics, Columbia University, 538 West 120th Street, New York, New York 10027, USA*

(Received 1 October 2004; published 3 December 2004)

We use the dynamical mean-field method to investigate electronic properties of heterostructures in which a finite number of Mott-insulator layers are embedded in a spatially infinite band insulator. The evolution of the correlation effects with the number of Mott insulating layers and with position in the heterostructure is determined, and the optical conductivity is computed. It is shown that the heterostructures are generally metallic, with moderately renormalized bands of quasiparticles appearing at the interface between the correlated and uncorrelated regions.

DOI: 10.1103/PhysRevB.70.241104

PACS number(s): 73.21.-b, 71.27.+a, 73.40.-c, 78.20.-e

An exciting direction in materials science is the fabrication and study of heterostructure involving “correlated electron” materials such as Mott insulators, high-temperature superconductors, and magnets.<sup>1,2</sup> The issues raised by these heterostructures, especially the variation with position of “correlated electron” properties, are of fundamental physical interest and would be crucial for prospective devices based on correlated electron compounds. Many interesting systems have been fabricated, including modulation-doped high- $T_c$  superconductors,<sup>3,4</sup> Mott-insulator–band-insulator heterostructures,<sup>5</sup> and a variety of combinations of magnetic transition-metal oxides,<sup>6–8</sup> but there has been relatively little theoretical study of the heterostructure-induced changes in many-body physics. The theoretical problem is difficult because it requires methods which can deal both with spatial inhomogeneity and strong correlation physics.

Despite the difficulties, several interesting works have appeared. Fang, Solovyev, and Terakura<sup>9</sup> used bulk band-structure calculations to gain insight into the effects<sup>6</sup> of strain fields induced by lattice mismatch in a heterostructure. Matzdorf and co-workers used band theory methods to study the surface electronic and lattice structure of  $\text{Sr}_2\text{RuO}_4$ .<sup>10</sup> Potthoff and Nolting, and Liebsch used dynamical-mean-field methods to study the consequences of the lower coordination at a surface,<sup>11–13</sup> and Freericks and co-workers studied a model system with uniform electron density and a spatially varying interaction parameter.<sup>14</sup>

All of these papers, however, treated situations in which the electronic density remained at the bulk value, and the physics arose from structural differences. A crucial feature of heterostructures is an inhomogeneous electron density caused by a spreading of charge across the interfaces which define the system. Recently,<sup>15,16</sup> we used realistic multi-orbital interaction parameters and a density-functional-theory-derived tight-binding band structure to model ground-state properties of the  $\text{LaTiO}_3/\text{SrTiO}_3$  heterostructure fabricated by Ohtomo *et al.*<sup>5</sup> While this study captured important aspects of the density inhomogeneity, it did not address the dynamical properties of correlated heterostructures. Further, this study employed the Hartree-Fock approximation, which is known to be an inadequate representation of strongly cor-

related materials, and in particular, does not include the physics associated with proximity to the Mott insulating state.

In this paper we use the dynamical-mean-field method,<sup>17</sup> which provides a much better representation of the electronic dynamics associated with strong correlations, to study the correlated electron properties of a simple Hubbard-model heterostructure inspired by—but not a fully realistic representation of—the systems studied in Ref. 5. We present results for observables including photoemission spectra, optical conductivity, and charge density, and highlight the similarities and differences to previous work.

We study a model of electrons moving on the  $B$  sites of an infinite  $(AA')\text{BO}_3$  perovskite lattice. The electronic Hamiltonian is  $H=H_{\text{band}}+H_{\text{int}}+H_{\text{coul}}$  with

$$H_{\text{band}} = -t \sum_{\langle ij \rangle, \sigma} (d_{i\sigma}^\dagger d_{j\sigma} + \text{H.c.}), \quad (1)$$

$$H_{\text{int}} = U \sum_i n_{i\uparrow} n_{i\downarrow} + \frac{1}{2} \sum_{i \neq j} \frac{e^2 n_{i\sigma} n_{j\sigma'}}{\epsilon |\vec{R}_i - \vec{R}_j|}, \quad (2)$$

Here,  $i$  labels the  $B$  sites so  $\vec{R}_i = (x_i, y_i, z_i) = a(n_i, m_i, l_i)$  with  $a$  the lattice constant. We include both an on-site ( $U$ ) and long-ranged Coulomb interaction: the screening field from the latter is important for the electron-density profile. We emphasize

$U \neq 0$  on all sites. We define the heterostructure by counterions of charge  $+1$  placed on a subset  $A'$  of the  $A$  sites. Here we study an  $n$ -layer  $[001]$  heterostructure defined by  $n$  planes of  $+1$  counterions placed at positions  $\vec{R}_j^{A'} = a(n_j + 1/2, m_j + 1/2, l_j + 1/2)$ , with  $-\infty < n_j, m_j < \infty$  and the  $l_j = 1, \dots, n$ . The resulting potential is

$$H_{\text{coul}} = - \sum_{i,j,\sigma} \frac{e^2 n_{i\sigma}}{\epsilon |\vec{R}_i - \vec{R}_j^{A'}|}. \quad (3)$$

Charge neutrality requires that the areal density of electrons is  $n$ . A dimensionless measure of the strength of the Coulomb interaction is  $E_c = e^2/(\epsilon a t)$ ; we choose parameters somewhat

arbitrarily so that  $E_c=0.8$  (this corresponds to  $t\sim 0.3$  eV and length  $a\sim 4$  Å and  $\varepsilon=15$ , which describe the system studied in Ref. 5). We found that the charge profile did not depend in an important way on  $\varepsilon$  for  $5 < \varepsilon < 25$ .

The basic object of our study is the electron Green's function, which for the [001] heterostructure may be written as ( $\vec{k}_\parallel$  is momentum in plane perpendicular to [001].)

$$G(z, z', \vec{k}_\parallel; \omega) = [\omega + \mu - H_{band} - H_{Coul} - \Sigma(z, z', \vec{k}_\parallel; \omega)]^{-1}. \quad (4)$$

We approximate the self-energy operator as the sum of a Hartree term arising from the long-ranged part of the Coulomb interaction,

$$\Sigma_H(z_i) = \sum_{j \neq i, \sigma} \frac{e^2 \langle n_{j\sigma} \rangle}{\varepsilon |\vec{R}_i - \vec{R}_j|}, \quad (5)$$

and a dynamical part  $\Sigma_D$  arising from local fluctuations. Following the usual assumptions of dynamical-mean-field theory (DMFT)<sup>17</sup> as generalized to inhomogeneous situations by Schwieger *et al.*,<sup>12</sup> we assume

$$\Sigma_D \Rightarrow \Sigma_D(z, \omega). \quad (6)$$

The layer ( $z$ )-dependent dynamical self-energy  $\Sigma_D$  is determined from the solution of a quantum impurity model<sup>17</sup> with the mean-field function fixed by the self-consistency condition

$$G^{imp}(z, \omega) = \int \frac{d^2 k_\parallel}{(2\pi)^2} G(z, z, \vec{k}_\parallel; \omega). \quad (7)$$

One must solve a separate impurity model for each layer, but the self-consistency condition [cf. Eq. (7)] implies that the solutions are coupled. It is also necessary to self-consistently calculate the charge density via  $n^{tot}(z) = -2 \int (d\omega/\pi) f_\omega \text{Im} G^{imp}(z, \omega)$  with  $f$  the Fermi distribution function. The numerics are time consuming, and it is therefore necessary to adopt a computationally inexpensive method for solving the quantum impurity models. We use the two-site method of Potthoff,<sup>18</sup> which reproduces remarkably accurately the scaling of the quasiparticle weight and lower Hubbard band near the Mott transition. We have also verified<sup>19</sup> that the two-site method reproduces within  $\sim 10\%$  the  $T=0$  magnetic phase diagram found by Ulmke<sup>20</sup> in a model with an unusual low-energy density-of-states peak.

Figure 1 shows the layer-resolved spectral function  $A(z, z; \omega) = -(1/\pi) \int [d^2 k_\parallel / (2\pi)^2] \text{Im} G(z, z, \vec{k}_\parallel; \omega + i0^+)$  for a 10-layer heterostructure with  $U=16t$  (about 10% greater than the critical value which drives a Mott transition in a bulk system described by  $H$  with  $n=\infty$ ). The spectral functions are in principle measurable in photoemission or scanning tunneling microscopy. Outside the heterostructure ( $z > 6$ ), the spectral function is essentially identical in form to that of the free tight-binding model  $H_{band}$ . The electron density is negligible, as can be seen from the fact that almost all of the spectral function lies above the chemical potential. As one approaches the heterostructure ( $z=6$ ), the spectral function be-

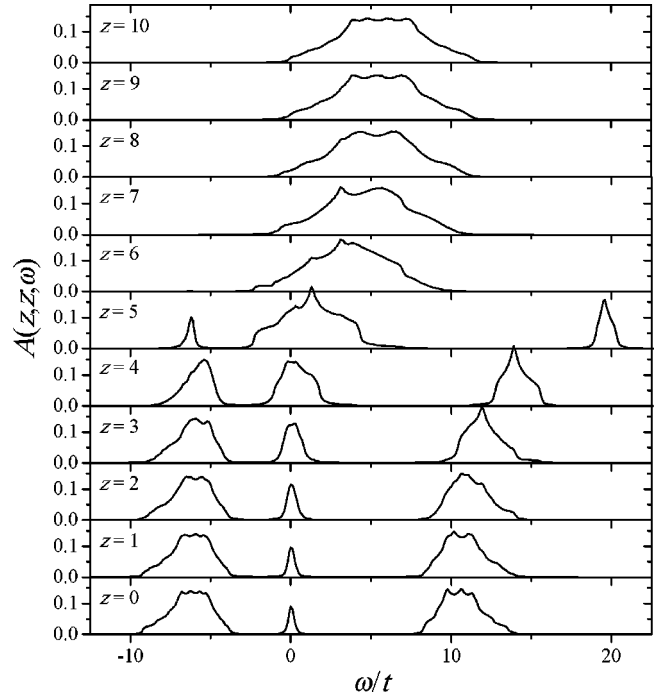


FIG. 1. Layer-resolved spectral function calculated for 10-layer heterostructure for  $U=16t$ ,  $\varepsilon=15$ . The heterostructure is defined by  $+1$  charges placed at  $z=\pm 0.5, \pm 1.5, \dots, \pm 4.5$  so the electronic ( $B$ ) sites are at integer values of  $z$ .

gins to broaden. Inside it ( $z \leq 5$ ) weight around  $\omega=0$  begins to decrease and the characteristic strong correlation structure of lower and upper Hubbard bands with a central quasiparticle peak begins to form. The sharp separation between these features is an artifact of the two-site DMFT [as is, we suspect, the shift in energy of the upper (empty state) Hubbard band for  $z=4, 5$ ]. Experience with bulk calculations suggests that the existence of three features and the weight in the quasiparticle region are reliable. Towards the center of the heterostructure, the weight in the quasiparticle band becomes very small, indicating nearly insulating behavior. For very thick heterostructures, we find the weight approaches 0 exponentially.

The behavior shown in Fig. 1 is driven by the variation in density caused by leakage of electrons out of the heterostructure region. Figure 2 shows as open squares the numerical results for the charge-density distribution  $n^{tot}(z)$  for the heterostructure whose photoemission spectra are shown in Fig. 1. One sees that in the center of the heterostructure ( $z=0$ ) the charge density is approximately one per site, and that there exists an edge region, of about three-unit-cell width, over which the density drops from  $\sim 1$  to  $\sim 0$ . The overall charge profile is determined mainly by the self-consistent screening of the Coulomb fields which define the heterostructure, and is only very weakly affected by the details of the strong on-site correlations (although the fact that the correlations constrain  $n^{tot} < 1$  is obviously important). To show this, we have used the Hartree-Fock approximation to recalculate the charge profile: the results are shown as filled circles in Fig. 2 and are seen to be almost identical to the DMFT results.

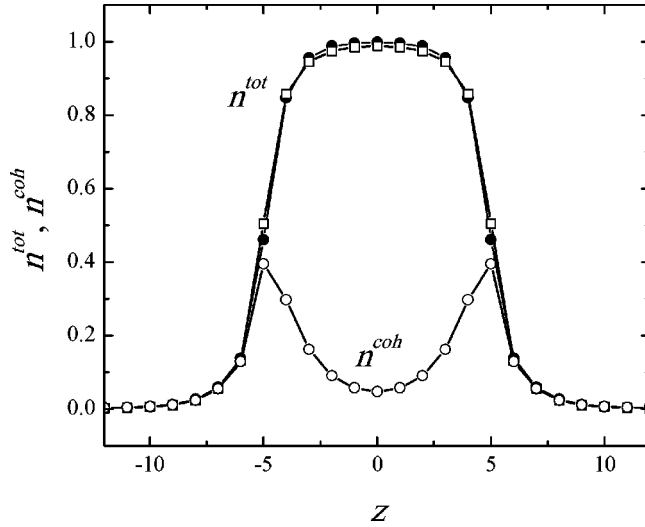


FIG. 2. Total charge density (open squares) and charge density from the coherent part near the Fermi level (open circles). For comparison, the total charge density calculated by applying the Hartree-Fock approximation to the Hamiltonian is shown as filled symbols. The parameters are the same as in Fig. 1.

The existence of an approximately three-unit-cell-wide edge region where the density deviates significantly from the values  $n^{tot}=0$  and 1 characteristic of the two systems in bulk form implies that only relatively thick heterostructures ( $n>6$ ) will display “insulating” behavior in their central layers, and suggests that the edge regions sustain quasiparticle subbands which give rise to metallic behavior. The open circles in Fig. 2 show the charge density in the “quasiparticle bands” [obtained by integrating  $A(z, z; \omega)$  from  $\omega=0$  down to the first point at which  $A(z, z; \omega)=0$ ]. One sees that these near-Fermi-surface states contain a small but non-negligible fraction of the total density, suggesting that edges should display relatively robust metallic behavior.

The results represent a significant correction to the Hartree-Fock calculation,<sup>16</sup> which leads, in the edge region, to a metallic quasiparticle density essentially equal to the total density.

The spectral function is determined by the layer-dependent, dynamical self-energy  $\Sigma_D(z, \omega)$ . In bulk materials one distinguishes Fermi liquid and Mott insulators by the low-frequency behavior of  $\Sigma_D$ ; in a Fermi liquid  $\Sigma_D \rightarrow_{\omega \rightarrow 0} (1-Z^{-1})\omega$  (leading to a quasiparticle with renormalized mass), while in a Mott insulator  $\Sigma_D \rightarrow_{\omega \rightarrow 0} \Delta^2/\omega$  (leading to a gap in the spectrum). In the heterostructures we study, we find that outside the high-density region, correlations are weak ( $Z \approx 1$ ), and that as one moves to the interior of thicker heterostructures, correlations increase ( $Z$  decreases). Mott insulating solutions ( $Z=0$ ) are never found; instead  $\Sigma_D(z, \omega) \sim [1-Z^{-1}(z)]\omega$  with  $0 < Z < 1$  for all layers  $z$ , although in the interior of thick, large  $U$  heterostructures  $Z$  is only nonvanishing because of leakage (quantum tunneling) of quasiparticles from the edges, and goes exponentially towards zero.

The nonvanishing  $Z$  indicates a Fermi-liquid state with well-defined coherent quasiparticles (thus negligible low-frequency scattering). In the heterostructure context the quasiparticles form subbands, with quasiparticle energies  $E_\alpha(\vec{k}_\parallel)$  and wave functions  $\varphi_\alpha[z; E_\alpha(\vec{k}_\parallel)]$ , which are the low-energy eigenfunctions and eigenvalues of

$$[Z^{-1}(z)E_\alpha\delta_{z,z'} + \mu - H_{band}(\vec{k}_\parallel) - H_{Coul}] \varphi_\alpha(z') = 0. \quad (8)$$

(We note that the two-site DMFT method used here is believed to give reasonable results for  $Z$  but of course neglects scattering effects. Near  $E_\alpha=0$  scattering is unimportant but of course will increase at higher energies.)

Numerical results for the coherent quasiparticles in a heterostructure with  $n=3$  and  $U=16t$  are shown in Fig. 3. For these parameters we find eight quasiparticle bands with non-

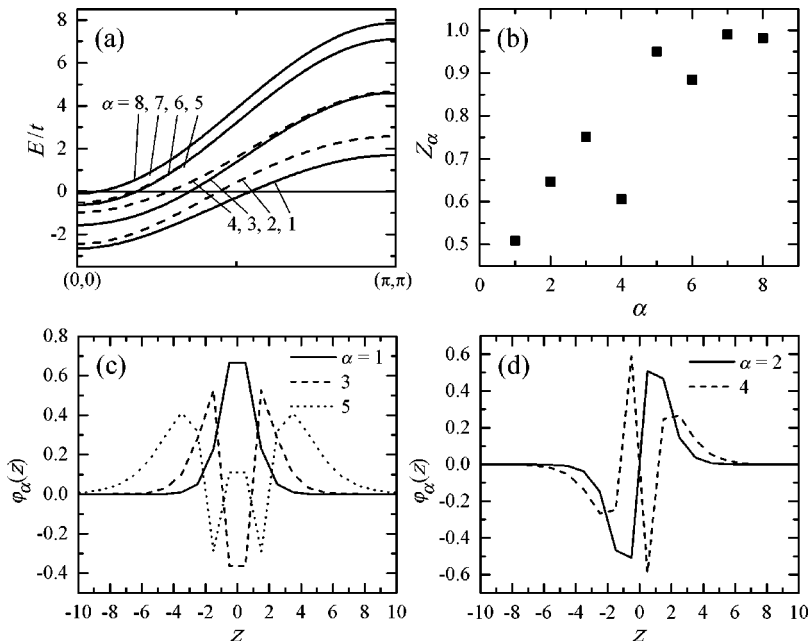


FIG. 3. (a) Dispersion relations of filled-subband quasiparticles calculated for three-layer heterostructure with  $U=16t$  and  $\varepsilon=15$ . The solid and broken lines are for odd and even  $\alpha$ , respectively. (b) Subband quasiparticle weights. (c,d) Quasiparticle wave functions for  $\alpha=1, 3, 5$  and  $2, 4$  at  $\omega=0$ . Here the heterostructure is defined by +1 charges placed at  $z=0, \pm 1$  so the electronic ( $B$ ) sites are at half integer values of  $z$ .

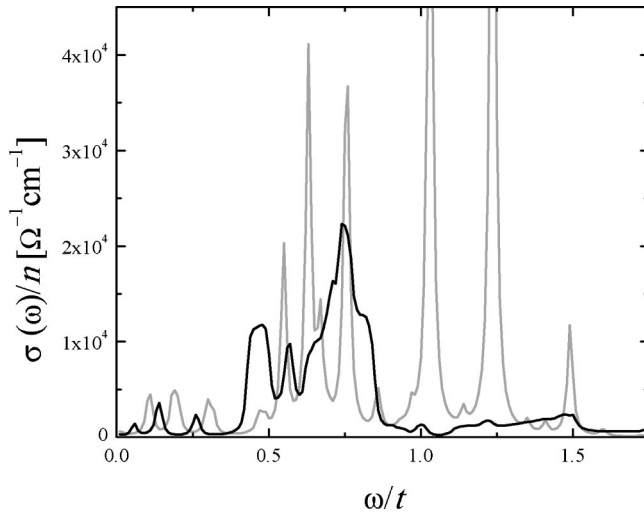


FIG. 4. Heavy lines: low-frequency (quasiparticle-region) optical conductivity for  $n=3$ ,  $U=16t$  heterostructure. Peaks arise from transition among subbands shown in Fig. 3(a). Light lines: conductivity calculated from Hartree-Fock approximation to same Hamiltonian.

vanishing electron density. The calculated dispersion relations are shown in panel (a) and are labeled  $\alpha=1, \dots, 8$  in order of decreasing electron density. We observe that the band splittings depend on momentum because of the layer dependence of  $Z$ . The corresponding quasiparticle weights  $Z_\alpha$  and real-space wave functions  $\varphi_\alpha(z)$  at  $\omega=0$  are shown in Figs. 3(b) and 3(c,d), respectively. (These quantities vary somewhat over the band also.)  $Z_\alpha$  is the smallest for the  $\alpha=1$  subband because its real-space wave function contains the largest weight at  $z=\pm 0.5$ , where the charge density is the largest and, therefore, the correlation effect is the strongest [see Fig. 3(c)].  $Z_\alpha$  generally increases with increasing  $\alpha$ , because as  $\alpha$  increases the wave-function amplitudes  $|\varphi_\alpha(z)|$  decrease in the high-density regions (near  $z=0$ ). The anomalies observed in  $Z_\alpha$  at  $\alpha=4, 6$  correspond to the increase of  $|\varphi_\alpha(z=\pm 0.5)|$  due to the symmetry of the wave function [see Fig. 3(d)].

The coherent subbands may be studied by optical conductivity with electric field directed along[001]. As an example,

the heavy line in Fig. 4 shows the quasiparticle contribution to the conductivity spectrum, calculated for a heterostructure with  $n=3$ ,  $U=16t$  and  $t=0.3$  eV using the standard Kubo formula with an optical matrix element obtained by applying the Peierls phase ansatz to  $H_{band}$ . Three main features are evident at  $\omega=0.75$ ,  $0.55$ , and  $0.45 t$ ; each of these has contributions from two interband transitions ( $1 \rightarrow 2$ ,  $2 \rightarrow 3$ ), ( $3 \rightarrow 4$ ,  $4 \rightarrow 5$ ), and ( $5 \rightarrow 8$ ,  $6 \rightarrow 7$ ), respectively. The optical features are not sharp because the quasiparticle band splitting depends on  $\vec{k}_\parallel$ . The weaker features at lower energies arise from transitions involving high-lying, only slightly occupied, bands. The lighter lines in Fig. 4 show the optical conductivity computed using the Hartree-Fock approximation. We see that the spectra are qualitatively similar, but that the Hartree-Fock absorption features occur at a larger energy because the  $Z$ -induced band narrowing is absent and are  $\delta$  functions, because in the Hartree-Fock approximation the subbands splittings are  $\vec{k}_\parallel$  independent.

To summarize, we have presented a dynamical-mean-field study of a “correlated electron heterostructure,” in which the behavior is controlled by the spreading of the electronic charge out of the confinement region. Our results show how the electronic behavior evolves from the weakly correlated to the strongly correlated regions, and in particular, confirms the existence of an approximately three-unit-cell-wide cross-over region in which a system, insulating in bulk, can sustain metallic behavior. We found that even in the presence of very strong bulk correlations, the metallic edge behavior displays a finite (roughly factor-of-2–3) mass renormalization. We showed how the magnitude of the renormalization is affected by the spatial structure of the quasiparticle wave function and determined how this renormalization affects physical properties, in particular, the optical conductivity. Important future directions for research include re-examination of the phase diagram using beyond Hartree-Fock techniques, and generalization of the results presented here to more complicated and realistic cases.

We acknowledge very fruitful discussions with M. Potthoff and H. Monien. This research was supported by the NSF under Grant No. DMR-00081075 (A.J.M.) and the JSPS (S.O.).

<sup>1</sup>M. Imada *et al.*, Rev. Mod. Phys. **70**, 1039 (1998).

<sup>2</sup>Y. Tokura and N. Nagaosa, Science **288**, 462 (2000).

<sup>3</sup>C. H. Ahn *et al.*, Science **284**, 1152 (1999).

<sup>4</sup>S. Gariglio *et al.*, Phys. Rev. Lett. **88**, 067002 (2002).

<sup>5</sup>A. Ohtomo *et al.*, Nature (London) **419**, 378 (2002).

<sup>6</sup>M. Izumi *et al.*, Mater. Sci. Eng., B **84**, 53 (2001), and references therein.

<sup>7</sup>A. Biswas *et al.*, Phys. Rev. B **61**, 9665 (2000).

<sup>8</sup>A. Biswas *et al.*, Phys. Rev. B **63**, 184424 (2001).

<sup>9</sup>Z. Fang *et al.*, Phys. Rev. Lett. **84**, 3169 (2000).

<sup>10</sup>R. Matzdorf *et al.*, Science **289**, 746 (2000).

<sup>11</sup>M. Potthoff and W. Nolting, Phys. Rev. B **60**, 7834 (1999).

<sup>12</sup>S. Schwieger *et al.*, Phys. Rev. B **67**, 165408 (2003).

<sup>13</sup>A. Liebsch, Phys. Rev. Lett. **90**, 096401 (2003).

<sup>14</sup>J. K. Freericks *et al.*, Phys. Rev. B **64**, 054511 (2001).

<sup>15</sup>S. Okamoto and A. J. Millis, Nature (London) **428**, 630 (2004).

<sup>16</sup>S. Okamoto and A. J. Millis, Phys. Rev. B **70**, 075101 (2004).

<sup>17</sup>A. Georges *et al.*, Rev. Mod. Phys. **68**, 13 (1996).

<sup>18</sup>M. Potthoff, Phys. Rev. B **64**, 165114 (2001).

<sup>19</sup>S. Okamoto and A. J. Millis (unpublished).

<sup>20</sup>M. Ulmke, Eur. Phys. J. B **1**, 301 (1998).